Supplementary Material: Total Air Content measurements from Renland

Sindhu Vudayagiri[1], Bo Vinther[1], Johannes Freitag[2], Peter L. Langen[3], Thomas Blunier[1]*,

1 Physics of Ice, Climate and Earth, Niels Bohr Institute, University of Copenhagen, Tagensvej 16, 2200 Copenhagen, Denmark
2 Alfred Wegner Institute, Snow and Firn Section Glaciology, 27570 Bremerhaven, Germany
3 Department of Environmental Science, iClimate, Aarhus University, Frederiksborgvej 399, 4000 Roskilde, Denmark
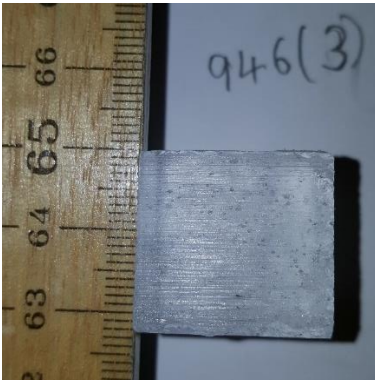
*Correspondence to: Thomas Blunier (blunier@nbi.ku.dk), Tel: +45 35 32 05 84

Contents

S1.   Typical sample at PICE

At PICE samples are cut into cubes of 2.2 x 2.2 x 2.4cm. The samples are then photographed, and the photographs are used to determine the mean bubble diameter of the sample. An example, sample of bag 946, in Fig. S1.

Figure S1: A cubical sample (2.2 x 2.2 x 2.4cm) cut out from ice core, photographed for bubble measurement.
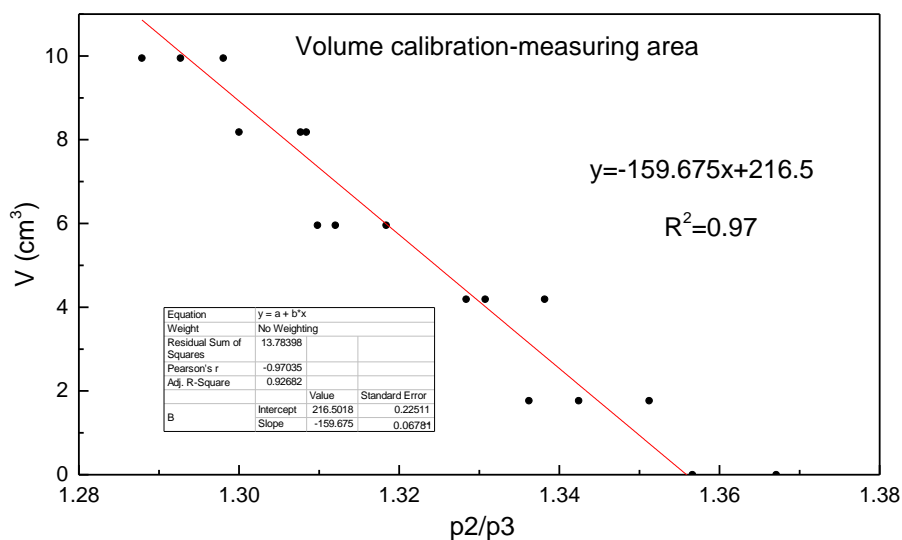
S2.   Calibration of the PICE set-up

The pressure of the captured air is measured with a Lektra P-BADR differential pressure gauge (DPG). The DPG is calibrated by attaching an absolute pressure gauge (APG) to the set-up following the procedure detailed in the thesis of Johanne Aagaard (2015).

The measuring volume (V_{ex}) must be determined accurately for precise TAC calculations. We follow the method developed by Schwander (1984) also described in Lipenkov (1995). For determining the V_{ex} precisely, steel balls of different known volumes (B) are placed in the extraction chamber, thereby changing the volume of the set-up. Dry air is admitted into the set up and is captured in the extra volume (V_{cyl}) with pressure P1. The rest of the set-up is evacuated. The air in V_{cyl} is then expanded to fill out V_{ex} and the pressure is noted as P2. Then the air is expanded to the entire volume of the set-up (V_t) with pressure noted as P3. The relation of these pressures and volumes lead to the following equation (S2).

$$B = V_t - V_{ex}\frac{P_2}{P_3} \tag{S1}$$

The pressures are measured with different combinations of steel balls in the extraction chamber (Fig. S2). From the linear regression, V_{ex} is determined as 159.68cm^3. The standard error of the regression gives an uncertainty of ±0.068cm^3 for V_{ex} and of ±0.225 cm^3 for V_t.

Volume calibration-measuring area

V (cm³) axis; p2/p3 axis

$y = -159.675x + 216.5$

$R^2 = 0.97$

Equation	y = a + b*x	
Weight	No Weighting	
Residual Sum of Squares	13.78398	
Pearson's r	-0.97035	
Adj. R-Square	0.92682	
	Value	Standard Error
B Intercept	216.5018	0.22511
B Slope	-159.675	0.06781

Figure S2: Volume Calibration: Volume (B) taken up by calibration volumes (steel balls) versus pressure ratio before and after expansion. The slope of the regression equals the size of the measuring volume.

S3.   SPIDER-System calibration

Careful calibration is essential for accurate sample measurement. Calibration here involved measuring the volume of the sampling lines and the effective temperature of the system (Fegyveresi, 2015). Both experiments made use of the ideal gas law relating pressure, volume, and temperature in the system. The volume of each of the 14 individual system lines ($V_{line(s)}$) was first experimentally determined. Steel plugs (inserts) with known volumes (~57 cm³, based on m_{steel} and ρ_{steel} for each plug) chosen to approximate ice samples, were inserted into each of the empty vessels (also with known volumes of ~96 cm³). An isothermal experiment for each of the vessels and lines individually was initiated, as follows: 1) gas pressure was measured in the vessel system line with the vessel valves closed; 2) the system was evacuated for 30 minutes, removing all air from the system lines ($< 4\times10^{-4}$ torr) while leaving air within the headspace of the vessel; 3) valves were then opened, allowing the headspace air to expand into the system lines where the final pressure (P_{final}) was measured. The volume of the line for each vessel (V_{line}) can then be determined from,

$$V_{line} = \frac{(V_{vessel} - V_{steel})(P_{initial} - P_{final})}{P_{final}}$$

(S2)

Laboratory temperatures may change by a few degrees from day to day and throughout the run due to excessive heat generated by the chiller. As the room temperature influences the temperature of the extraction manifold and GC sample loop, we need to determine the effective temperature of the line when air samples are analysed. To calibrate this, three expansion experiments were run for each vessel individually, with the vessel held at -70°C as during sampling, and with the room temperature at 24.05, 28.45, and 31.35°C. Each of these three runs for each vessel yielded an effective temperature (T_{eff}),

$$T_{eff} = \frac{P_{final}(V_{head} - V_{line})T_{initial}}{P_{initial}V_{head}} \tag{S3}$$

Substituting V_{head} for V_{vessel}- V_{steel} yields,

$$T_{eff} = \frac{P_{final}(V_{vessel} - V_{steel} + V_{line})T_{initial}}{P_{initial}(V_{vessel} - V_{steel})} \tag{S4}$$

Linear regressions for T_{eff} versus room temperature for each vessel was calculated, and these equations were then used with measured room temperature when the sample was expanded into the manifold to reduce sample data to standard temperature and pressure (STP; Eqs. S5 and S6).

$$V_{STP} = \left(\frac{P_{final}V_{final}}{T_{eff}}\right)\left(\frac{T_{STP}}{P_{STP}}\right) \tag{S5}$$

$$TAC = \frac{V_{STP}}{m_{ice}} \tag{S6}$$

For further detailed information on the calibration of the SPIDER extraction device, refer to the thesis of John M. Fegyveresi (Fegyveresi, 2015).

For $\delta^{15}N$ the measurement procedure is similar. However, the samples are only 13g on average. Given the relative to the sample big headspace makes the solubility correction obsolete.

S4. Cut bubble correction

The cut bubble effect (CBE) calculates from the average bubble diameter $\langle D \rangle$ in the sample and sample surface area A_S and volume V_S, respectively (Martinerie et al., 1990). The calculation assumes spherical bubbles.

$$CBE = \frac{TAC - TAC_{raw}}{TAC} = \frac{1}{2}\langle D \rangle \frac{A_S}{V_S} \tag{S7}$$

CBE corrected total air content (TAC) then calculates from the TAC_{raw}

$$TAC = (1 - CBE)^{-1} \cdot TAC_{raw} \tag{S8}$$

Samples measured at PICE are corrected individually. Individual bubble diameters have not been measured for samples measured at PSU. Those measurements are a by-product of CH_4 concentration and $\delta^{15}N$ measurements. Bubble diameters are estimated from the PICE data. The bubble diameter decreases linearly from 120 to 530 m below surface (Fig S3). For the corresponding sample range in the PSU data (from the surface to the YD-Preboreal transition at 532.6m below surface) we calculate the bubble diameter from the linear regression of the PICE data. The one sigma prediction interval has an uncertainty of 0.07mm. The bubble diameter below 530 m is very variable, and we apply the average bubble size of the PICE data (N = 88) which is 0.362 mm ± 0.114 mm (one sigma standard deviation). The resulting cut bubble effect (CBE) depends on the size and shape of the sample. Samples from PSU-CH_4 measurements are cylindrical with diameter 4.1 cm, height of 5.5±0.3 cm, and weighing 65 ± 3 g each. PSU-$\delta^{15}N$ samples are smaller cubes of 20 x 12 x 50 mm weighing 13 g. Averaged CBE corrections in table S1.

	Upper section (down to 532.6m)	Lower section
PSU-CH$_4$ samples	1.7±0.5%	2.4±0.8%
PSU-δ^{15}N samples	4.2±1.1%	5.6±1.8%

Table S1: Average CBE corrections for the different sections and samples of the PSU data.
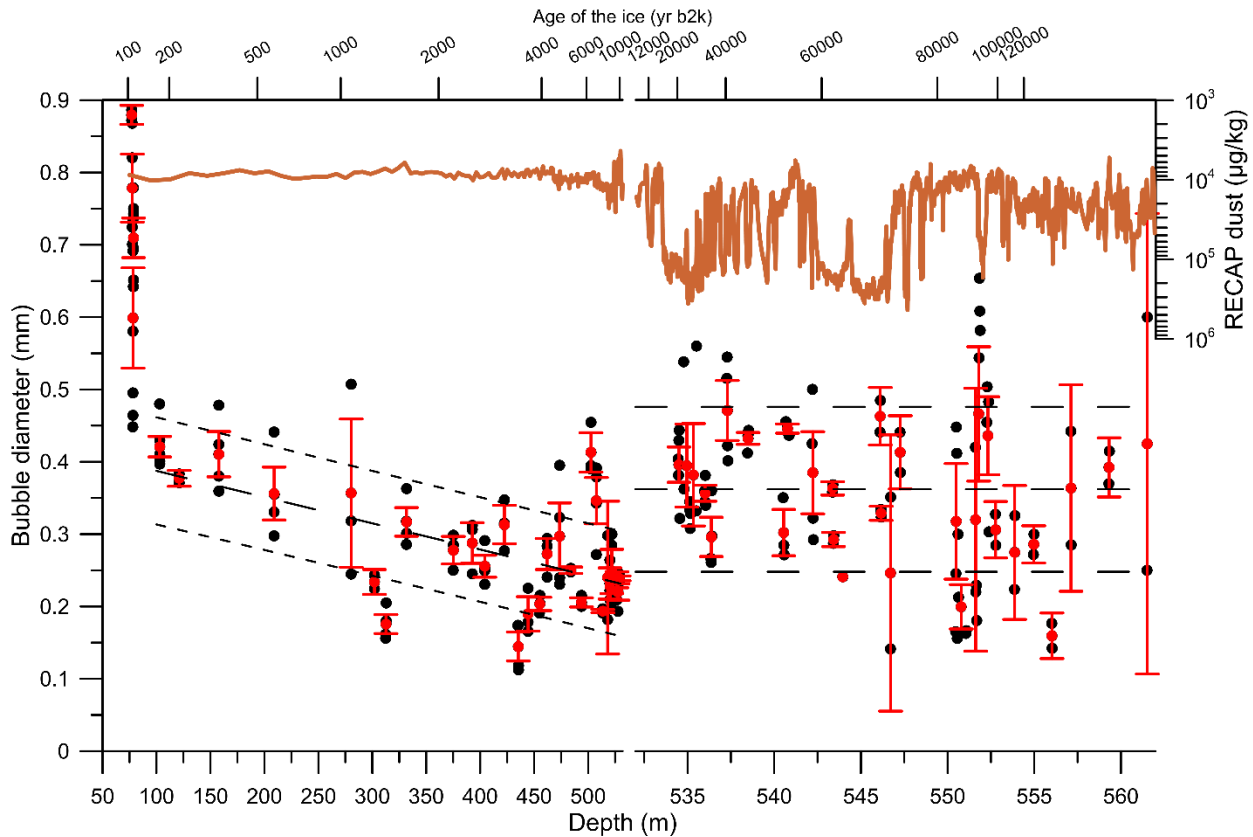
Figure S3: Bubble diameter of the PICE samples versus depth. Black dots are individual samples. Red dots with error bars are averages for samples within one bag (0.55cm) with standard errors of the mean. Dotted lines are error estimates for the correction of the PSU samples. Black line RECAP dust record for orientation (Simonsen et al., 2018). Top axis is the ice time scale for the RECAP core (Simonsen et al., 2018).

S5.   Agreement between datasets

At PICE, the air from the ice samples is extracted with two melt-freeze cycles and is stripped off its moisture before its pressure is measured. The extraction process at PSU has only one melt-freeze cycle and there is no water vapor trap leading to considerable uncertainty due to the added partial pressure of the moisture and CBE is estimated from the PICE measurements.

To assess the quality of the data sets, we present correlation plots between the PSU and the PICE datasets. Figure S4 shows average values for the two PSU datasets versus their closest, (within one meter) correspondent in the PICE dataset. Samples that have no correspondent within 1 meter distance are excluded. Offsets of individual samples can be large. However, we observe no systematic offset between the datasets.
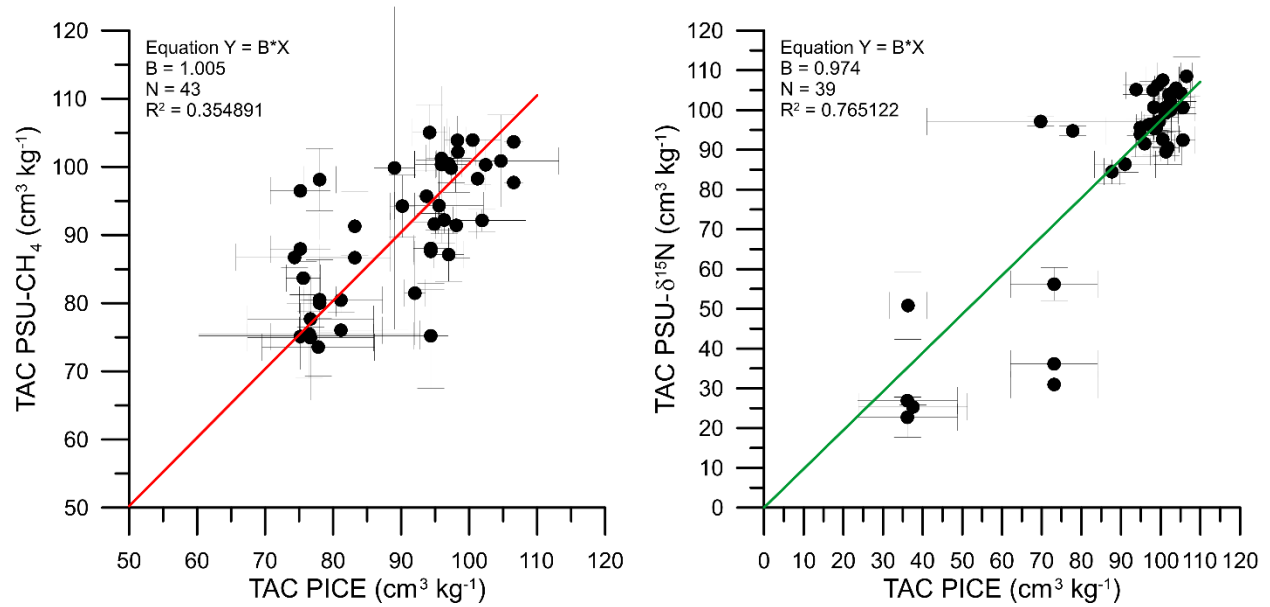
Figure S4: Correlation of PSU and PICE TAC data. Plotted are the closest PICE neighbours (within one meter) to the PSU TAC data obtained during the CH_4 and $\delta^{15}N$ measurements on the left- and right-hand side, respectively. Uncertainties are standard errors of the mean data.

S6. Time scale

We are making use of the RECAP GICC05 ice age scale (Simonsen et al., 2018). The time scale is based on counting annual layers in the upper section and by tie points to other Greenland ice cores in deeper strata (see Simonsen et al., 2018 for details). The gas time scale is younger by Δage, which is variable depending on temperature and accumulation rate.

Firn air measurements from RECAP show the kink in the CO_2 and $\delta^{15}N$ records indicating the close off depth at about 55.5 m below surface. This results in a shallow Δage of only about 75 years which we use for presenting the Holocene part of the record on the gas time scale.

Based on matching Dansgaard-Oeschger events in the water isotopes to their corresponding CH_4 signal, Δage in the depth range 535 to 546 m is on the order of 400 years.

S7. Theoretical present-day TAC with 0% and 100% melt layers

S7.1. Theoretical present-day TAC of ice unaffected by melt at Renland ice cap

Unfortunately, no data is available for the present day annual mean pressure at the Renland ice cap. Therefore, we calculate it by applying the barometric formula (equation 2). The closest measurement station is Illoqqortoormiut which we use as the reference station with $T_a = 265.5°K$, $h_a = 0$ m, $P_a = 1012.2$ mbar (Cappelen et al., 2001). We use the Renland bore hole temperature $T_c = 255°K$, $h_c = 2315m$, $M_{air} = 0.028964$ kg/mol. The present day annual mean lapse rate can be calculated from the temperatures at Renland and Illoqqortoormiut, respectively to -4.5 K km^{-1}. The average pressure then calculates to 747 mbar. We calculate the pore volume V_c according to Martinerie et al. (1994)

at T_c = 255°K to 134 cc kg⁻¹. TAC then calculates (equation 1) to 99 cm³ kg⁻¹ at standard temperature and pressure. This value compares well to the TAC measured for the last 2000 years (depth range 76.6 - 345.7 m, Fig. S5).
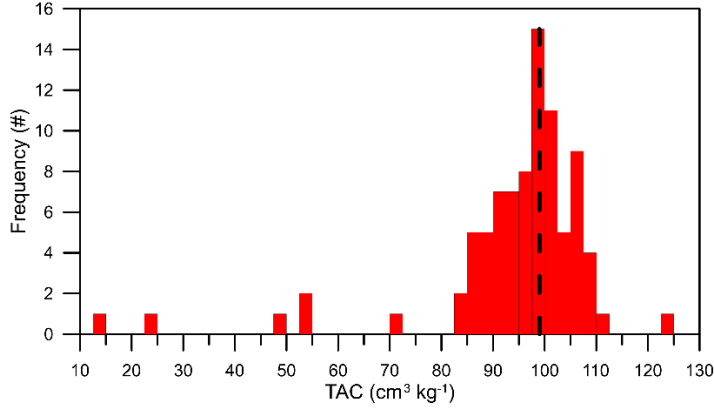

Figure S5: TAC of individual samples in the depth range 76.6 to 345.7m covering the last 2000 years. Note samples with known melt features are included. Black hashed line indicates the theoretical calculated air content of 99 cm³ kg⁻¹.

S7.2. Theoretical present-day TAC in a 100% melt sample at the Renland ice cap

For this calculation we assume that the melt water of the sample is in equilibrium with the atmosphere and then freezes instantly. To compute the amount of air dissolved in water at 273K and at an atmospheric pressure of 747 mbar, Henry's solubility law will be used (Sander, 2015).

Temperature dependence of Henry's constant,

$$H^{cp}(T) = H_{\Theta}^{cp} \times exp\left[\frac{-\Delta_{sol}H}{R}\left(\frac{1}{T} - \frac{1}{T^0}\right)\right]$$

The concentration of gas dissolved in mol m⁻³ calculates to $C_a = H_{\Theta}^{cp} \times P$, where P is the partial pressure of the species in the gas phase at equilibrium conditions, in this case on Renland.

TAC for an individual gas calculates as $TAC = \frac{C_a \times R \times T_0}{\rho_{H2O} \times p_0}$, with T_0 = 273.15 K and p_0 = 1013mbar.

Gas	H_{Θ}^{cp} $(\frac{mol}{Pa.m^3})$ (Θ = 298.15 K)	$\frac{-\Delta_{sol}H}{R}$ (K)	C_a $(\frac{mol}{m^3})$ at 273 K	C_a $(\frac{mol}{m^3})$ at 275 K
O_2	1.3×10^{-5}	1700	0.344	0.328
N_2	6.4×10^{-6}	1600	0.617	0.591
			TAC 21.5 cc kg⁻¹	**TAC 20.6 cc kg⁻¹**

From the theoretical TAC calculations for no melt and 100% melt at present day Renland we obtain: %-melt = $-1.291 \cdot TAC$ $(cc$ $kg^{-1}) + 127.819$ (Figure S6). Samples from bag no. 143 of the RECAP ice core were cut so that they have approximately 50% and 100% melt. This approach has obviously a large uncertainty. Nevertheless, the results are also shown in Fig. S6, validating our theoretical approach.
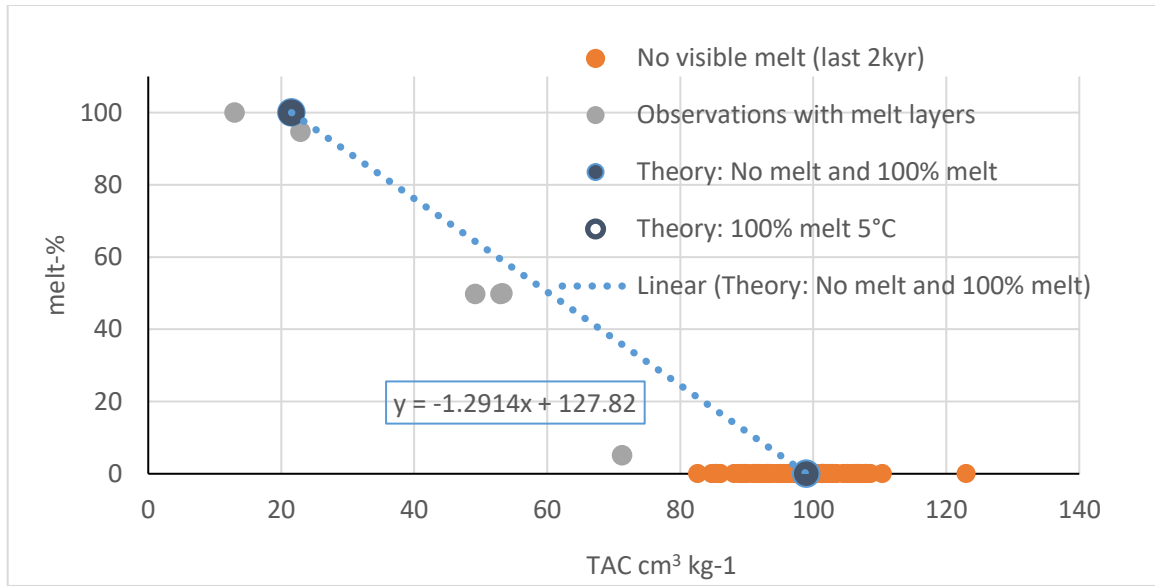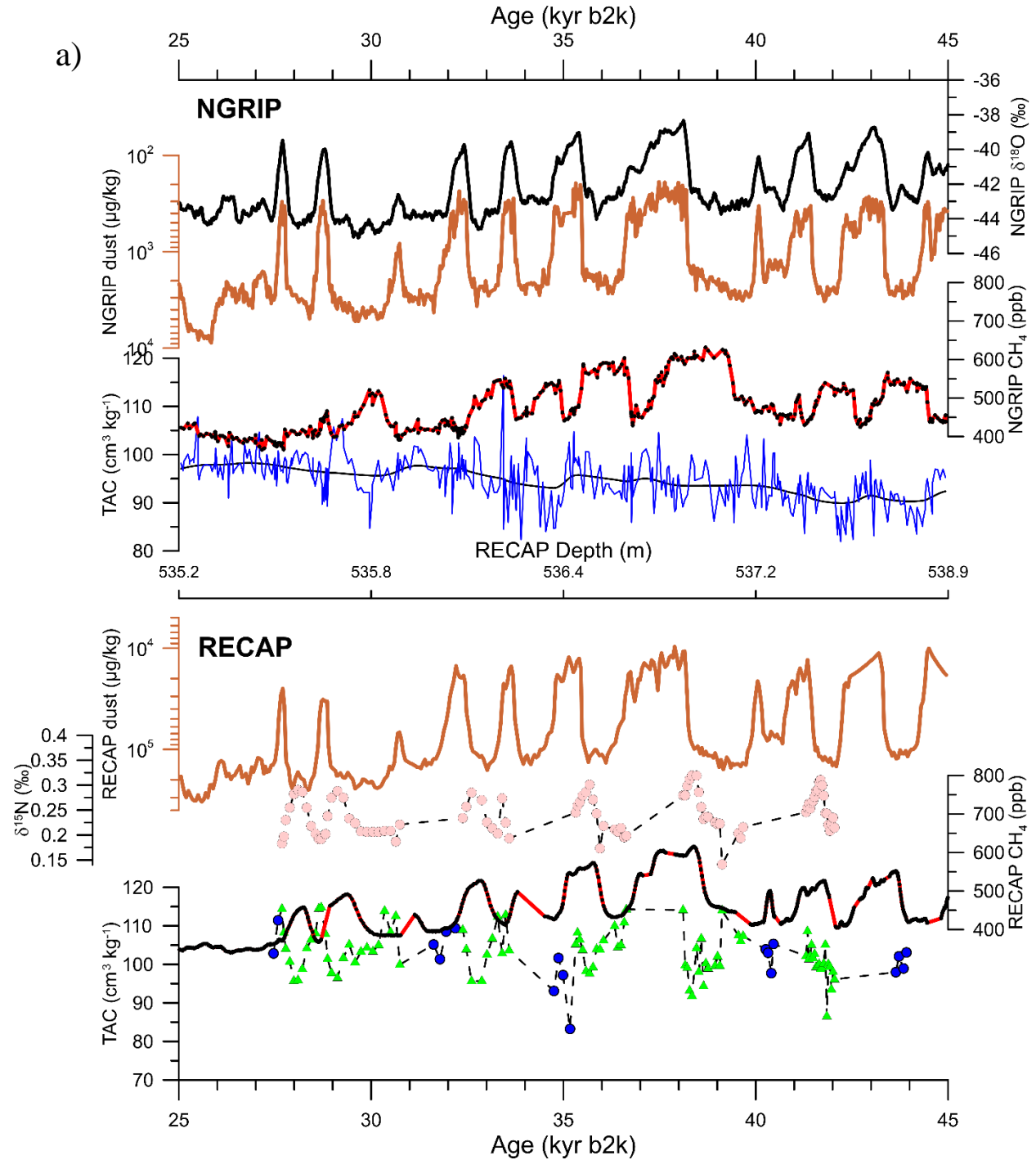
7

Figure S6: Data and theoretical values for TAC with varying contributions from melt layers.
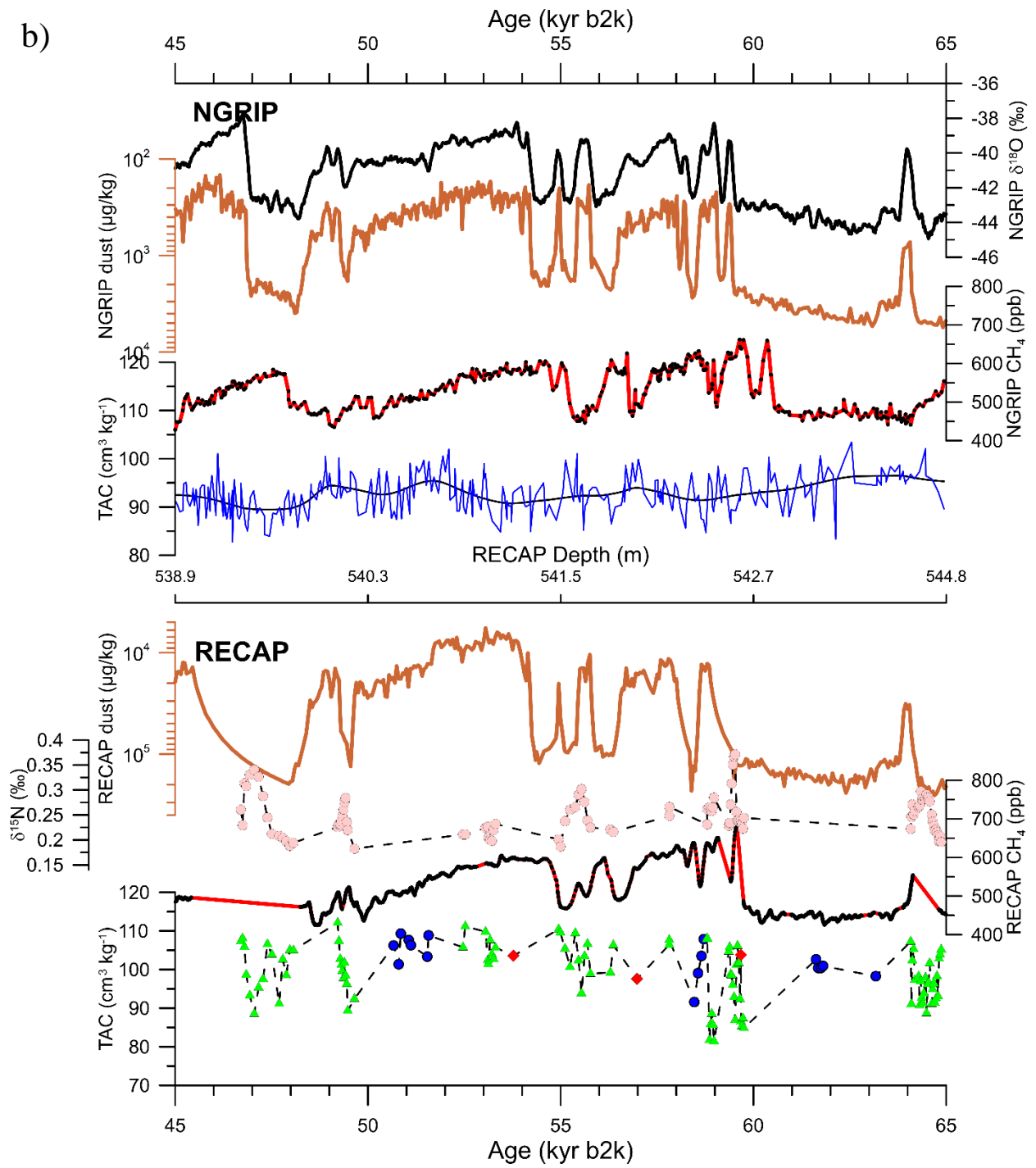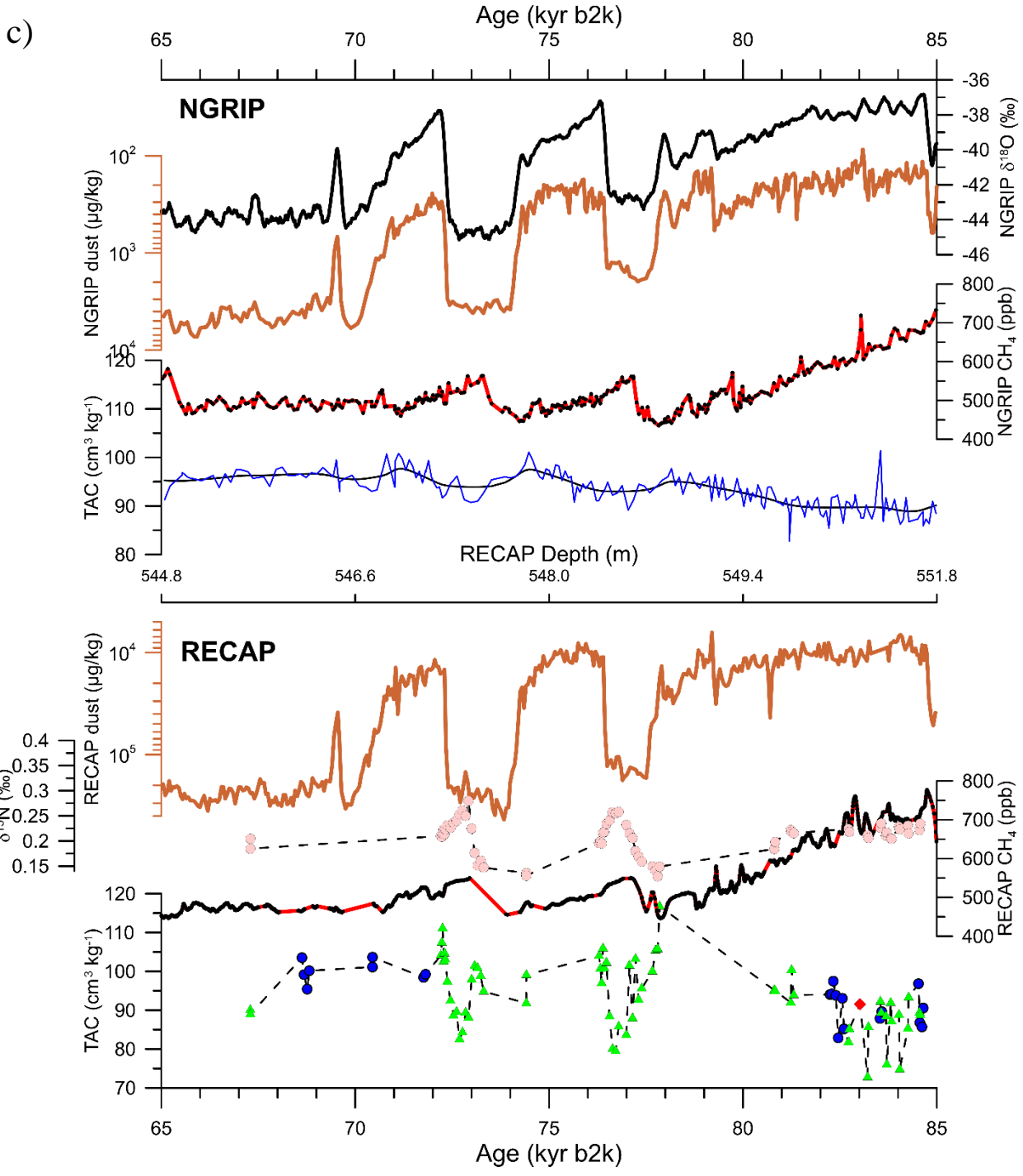
S8.   The glacial record of RECAP and NGRIP

The records are presented in 4 sections 25-45, 45-65, 65-85, and 85-105 kyr b2k.
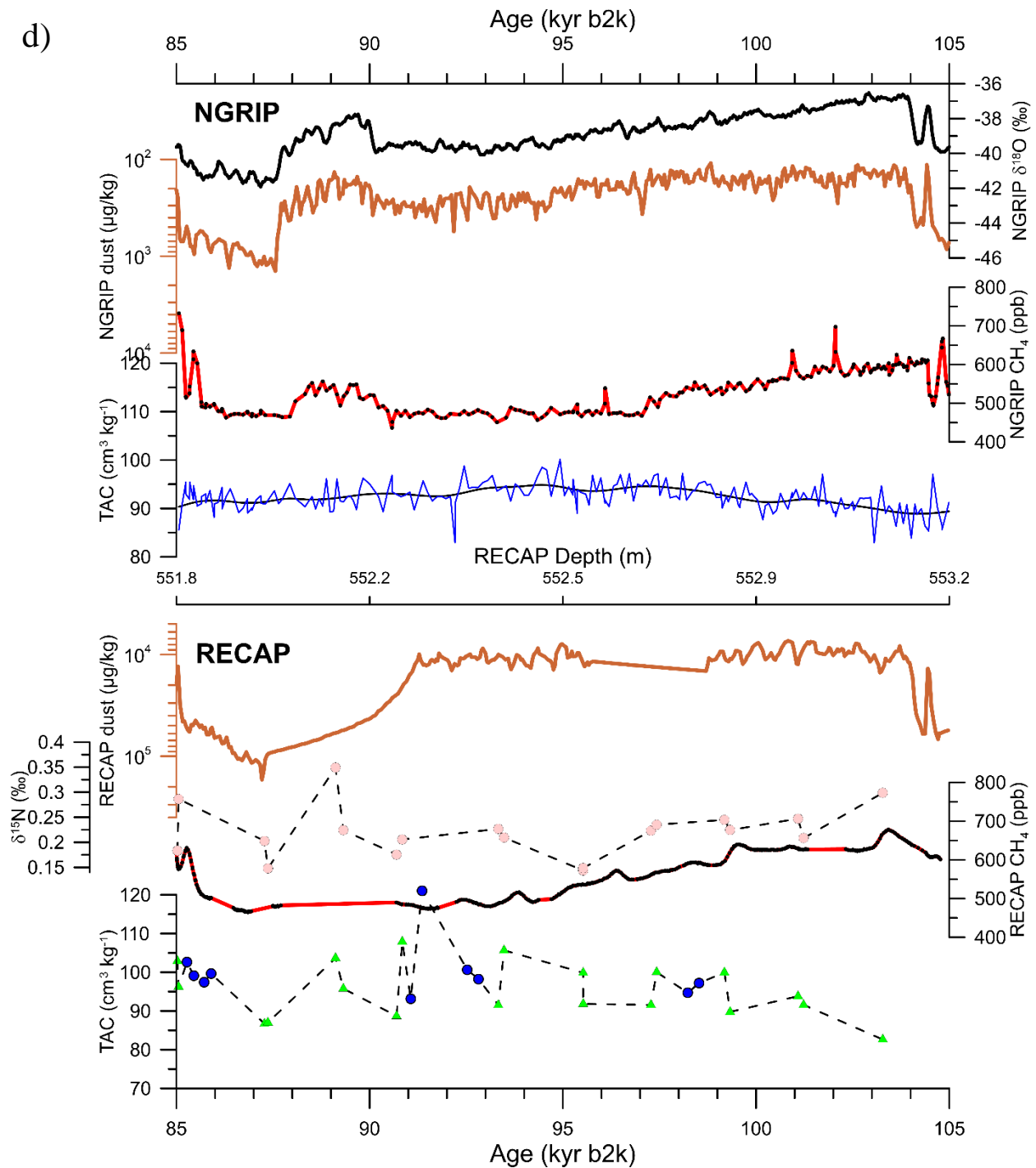
b)

NGRIP

RECAP

c)

NGRIP

RECAP

Figure S7a to d: Glacial records from RECAP and NGRIP: NGRIP top to bottom: water isotopes (black) (North Greenland Ice Core Project members, 2004), inverted dust (red) (Ruth et al., 2007), CH$_4$ (black dots and red line) (Baumgartner et al., 2014), TAC (blue line and spline fit in black) (Eicher et al., 2016). RECAP top to bottom inverted dust (red), $\delta^{15}N$ (pink), on-line CH$_4$ (black dots and red line, note that this data is not fully calibrated, concentrations are not absolute), TAC (TAC from PICE, PSU-CH$_4$, and PSU-$\delta^{15}N$ as blue dots, red diamonds, and green triangles, respectively).

S8.1.   Variations associated with DO-events

We stacked the TAC data over DO events to see the general features of the events. We did the same with the methane data and the δ^{15}N data. As lined out in the main text, dynamical effects in TAC can be expected from the moment of change till a new steady state is established. For the firn column this is when at a DO event the higher accumulation snow has reached close off. As methane and temperature changes have been found to happen in close timely proximity, the depth interval to be considered for a dynamical change is between the depth when methane changes are observed and the depth where changes in parameters recorded in the ice occur, e.g δ^{18}O of H_2O or dust. For the RECAP ice core, we find that this depth interval corresponding to Δage is quite variable. Why this is the case we ignore. We chose to produce a stacked plot over DO events with normalized time axis. For each event the time axis is normalized so that the methane transition (in some events defined by change in δ^{15}N) is set to 1 and the decrease in dust (coincident with the change in δ^{18}O) is set to 0. We treat the Eicher et al. (2016) dataset for NGRIP in a similar way. Note: We used the NGRIP Δage to define the start of the methane increase. However, since Δage references the midpoint of the transition we have assigned a value of 0.9 to the midpoint of the methane increase to make the NGRIP analyses compatible with our approach for RECAP. Figures S8a and S8b show the result of this exercise for RECAP and NGRIP, respectively. For TAC, methane and δ^{15}N, a lowpass cubic spline fit with a 200-year cutoff period, according to Enting (1987) with 1 sigma uncertainties for the spline fit is shown. Individual measurements for TAC (RECAP and NGRIP) and δ^{15}N (RECAP only) are plotted colour coded for the different DO events. For RECAP open symbols indicate events that were excluded for the analyses where we have less than 10 TAC measurements for the event.

Methane data was also stacked and splined in a similar way. Apart from potential tiny modulations occurring in the trapping process the methane record of NGRIP and RECAP must be identical. However, the RECAP data has been analyzed in a continuous flow setup resulting in smoothing of this highly compressed record. Nevertheless, the start of the events in CH_4 can be clearly identified. Note that this smoothing only applies to the RECAP CH_4 data. All other data are individual samples that do not suffer from smoothing effects during the analyses.
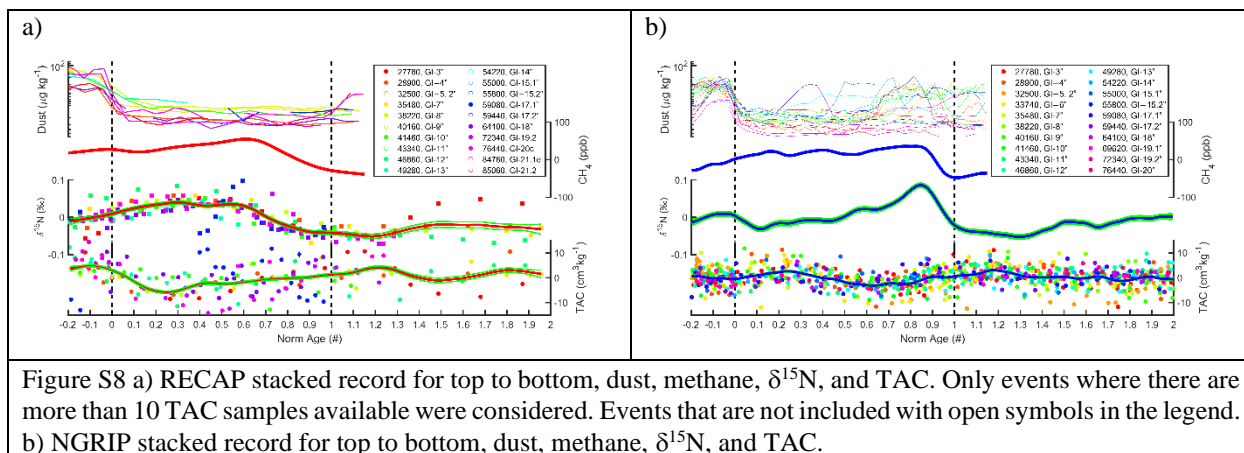
Figure S8 a) RECAP stacked record for top to bottom, dust, methane, $\delta^{15}N$, and TAC. Only events where there are more than 10 TAC samples available were considered. Events that are not included with open symbols in the legend. b) NGRIP stacked record for top to bottom, dust, methane, $\delta^{15}N$, and TAC.

S9.   TAC and insolation

Following Eicher (2016 , and references therein) we calculate the correlation between TAC and insolation. Like previous authors we chose an integrated local summer insolation (ISI) defined as the sum of insolation where the daily insolation exceeds 380 Wm^{-2}. While Raynaud et al. (2007) find high correlation of r^2 of 0.86 for Antarctic sites. The correlation for NGRIP is only 0.03 (Eicher et al., 2016). For RECAP the correlation becomes only 0.004 (Figure SX) which leads us to speculate that the insolation effect may be depending on the accumulation rate. However, the higher variability associated with D-O events may explain part of the observed lower correlation.
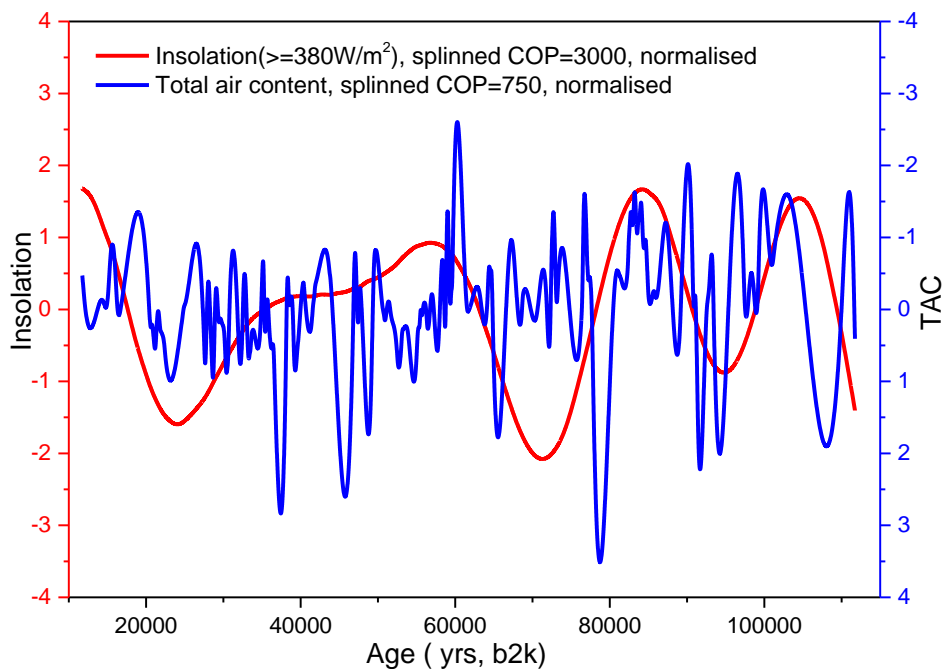

Figure S9: Insolation ($\geq$ 380 W/m^2) signal for Renland, splined (COP=3000) and normalized in red, Glacial TAC signal of Renland core, splined (COP=750) and normalized in blue. The correlation of these signals is r^2=0.004.

S10.   Elevation calculations

Handpicked sections where we believe the climate at RECAP is stable enough to calculate elevation from TAC. Those are the Last Glacial Maximum, GS-18, GS-19.1, and GI-23.1.
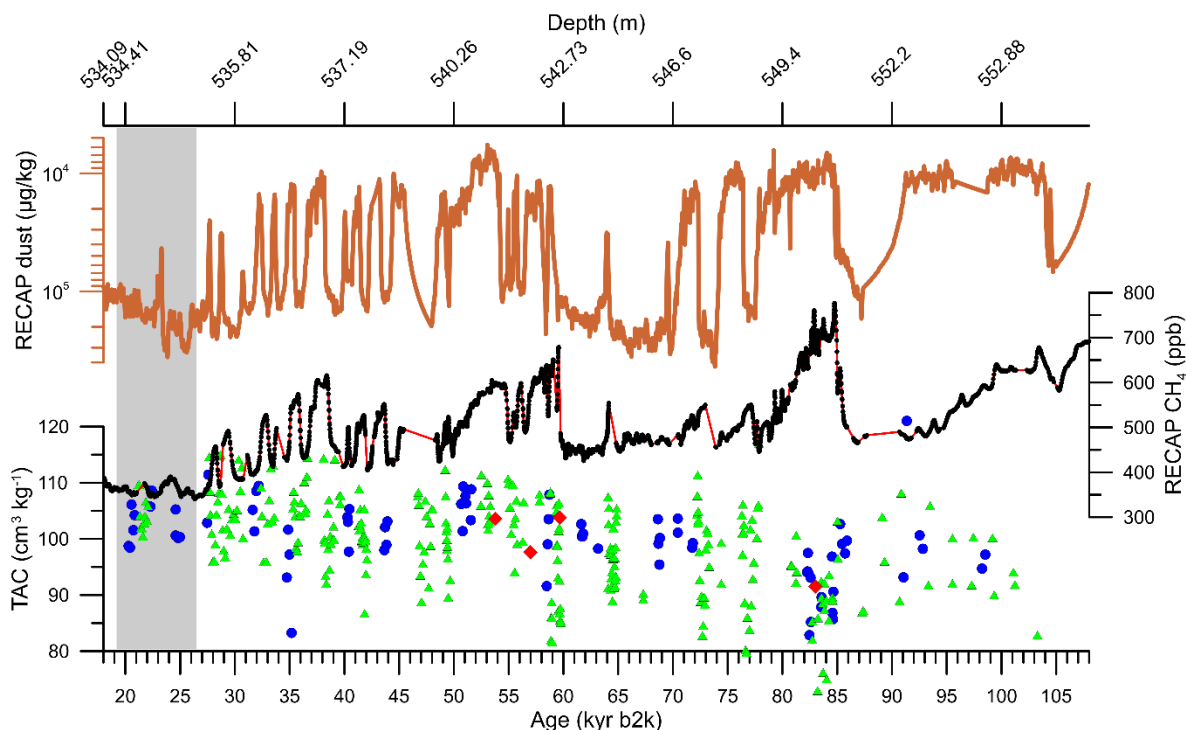

Figure S10: Top to bottom: RECAP inverted dust (red), on-line CH_4 (black dots and red line, note that this data is not fully calibrated, concentrations are not absolute), TAC (TAC from PICE, PSU-CH_4, and PSU-$\delta^{15}N$ as blue dots, red diamonds, and green triangles, respectively). Gray sections indicate the area that we use to calculate ice sheet elevation from TAC.

References:

Aagaard, J.: Measurements of total air content of ice from EUROCORE, Greenland, Master thesis, Niels Bohr Institute, Faculty of Science, University of Copenhagen, 76 pp., 2015.

Baumgartner, M., Kindler, P., Eicher, O., Floch, G., Schilt, A., Schwander, J., Spahni, R., Capron, E., Chappellaz, J., Leuenberger, M., Fischer, H., and Stocker, T. F.: NGRIP CH_4 concentration from 120 to 10 kyr before present and its relation to a $\delta^{15}N$ temperature reconstruction from the same ice core, Clim Past, 10, 903-920, 10.5194/cp-10-903-2014, 2014.

Cappelen, J., Jørgensen, B. V., Laursen, E. V., Stannius, L. S., and Thomsen, R. S.: The Observed Climate of Greenland , 1958-99 - with Climatological Standard Normals , 1961-90 Klimaobservationer i Grønland , 1958-99, Danish Meteorological Institute, CopenhagenISSN 1399-1388, 151, 2001.

Eicher, O., Baumgartner, M., Schilt, A., Schmitt, J., Schwander, J., Stocker, T. F., and Fischer, H.: Climatic and insolation control on the high-resolution total air content in the NGRIP ice core, Clim. Past, 12, 1979-1993, 10.5194/cp-12-1979-2016, 2016.

Enting, I. G.: On the use of smoothing splines to filter CO_2 data, J Geophys Res-Atmos, 92, 10977-10984, 10.1029/JD092iD09p10977, 1987.

Fegyveresi, J. M.: Physical properties of the West Antarctic Ice Sheet (WAIS) Divide deep core: Development, evolution, and interpretation, Ph.D. thesis, Department of Geosciences, The Pennsylvania State University, Ann Arbor, 304 pp., 2015.

Lipenkov, V., Candaudap, F., Ravoire, J., Dulac, E., and Raynaud, D.: A New Device for the Measurement of Air Content in Polar Ice, Journal of Glaciology, 41, 423-429, 1995.

Martinerie, P., Lipenkov, V., and Raynaud, D.: Correction of air content measurements in polar ice for the effect of cut bubbles at the surface of the sample, Journal of Glaciology, 36, 299-303, Doi 10.3189/002214390793701282, 1990.

Martinerie, P., Lipenkov, V. Y., Raynaud, D., Chappellaz, J., Barkov, N. I., and Lorius, C.: Air content paleo record in the Vostok ice core (Antarctica): A mixed record of climatic and glaciological parameters, J Geophys Res-Atmos, 99, 10565-10576, 10.1029/93jd03223, 1994.

North Greenland Ice Core Project members: High-resolution record of Northern Hemisphere climate extending into the last interglacial period, Nature, 431, 147-151, 10.1038/nature02805, 2004.

Raynaud, D., Lipenkov, V., Lemieux-Dudon, B., Duval, P., Loutre, M. F., and Lhomme, N.: The local insolation signature of air content in Antarctic ice. A new step toward an absolute dating of ice records, Earth Planet Sc Lett, 261, 337-349, 10.1016/j.epsl.2007.06.025, 2007.

Ruth, U., Bigler, M., Röthlisberger, R., Siggaard-Andersen, M.-L., Kipfstuhl, S., Goto-Azuma, K., Hansson, M. E., Johnsen, S. J., Lu, H., and Steffensen, J. P.: Ice core evidence for a very tight link between North Atlantic and east Asian glacial climate, Geophys Res Lett, 34, 10.1029/2006GL027876, 2007.

Sander, R.: Compilation of Henry's law constants (version 4.0) for water as solvent, Atmos. Chem. Phys., 15, 4399-4981, 10.5194/acp-15-4399-2015, 2015.

Schwander, J.: Lufteinschluss im Eis von Grönland und der Antarktis, PhD thesis, Universität Bern, 1984.

Simonsen, M. F., Cremonesi, L., Baccolo, G., Bosch, S., Delmonte, B., Erhardt, T., Kjær, H. A., Potenza, M., Svensson, A., and Vallelonga, P.: Particle shape accounts for instrumental discrepancy in ice core dust size distributions, Clim. Past, 14, 601-608, 10.5194/cp-14-601-2018, 2018.